Scattering from spheres and cylinders - revisited

Halvor Hobæk and Tonje Lexau Nesse

Department of Physics and Technology, University of Bergen, Allegt. 55, N5007 Bergen, Norway

Abstract. Backscattering of sound from elastic spheres is commonly applied for calibration of acoustic systems. Measurements on the "form function" of various tungsten carbide spheres turned out not to match simulations based on standard theory and elastic parameters found in the literature. This initiated a search for better parameters. One method for determining the parameters is presented, and the results compared to previously published parameters. It is found that for accurate calibration purposes it is not sufficient to use nominal values for the material, since the actual values may vary from batch to batch and between different manufacturers. Also the suspension method of the spheres turns out to be critical.

Measurements on short cylinders of aluminum rotated in the sound beam reveal the presence of two sets of strong lobes in addition to ordinary sidelobes caused by the finite cylinder length. Analysis of these lobes indicates that they are caused by Lamb-type waves excited in the cylinder. Dispersion diagrams obtained from the measurements are presented for the two relevant wave modes.

PACS: 43.20.El, 43.20.Fn, 43.20.Gj, 43.40.Fz, 43.58.Vb.

INTRODUCTION

During the set up of an experiment to study scattering from fish backbones it was decided to use spheres for testing and calibration. It was then discovered that the measured scattering did not match the expected frequency response computed using standard formulas and parameters. The need for better parameters to describe the form function of the tungsten carbide (WC) spheres that were used led to a procedure for inverting the measured form function.

At a later stage in the experiment also short aluminum cylinders were used as targets. These were rotated about a vertical axis with the cylinder axis and sound beam horizontal. It was found that at about 18 degrees away from broadside direction (in a monostatic mode) there is a strong lobe in the scattered signal, almost independent of frequency. Another lobe is found to be strongly dependent on frequency and appears only at frequencies above a certain threshold frequency. So far we have not found observations of such lobes described in the literature. The lobes are interpreteded as due to waves propagating in the cylinder. From the measurements dispersion relations for these waves are obtained. It appears that they are related to symmetric and asymmetric Lamb waves excited in the cylinder.

The organization of the paper is as follows. After a brief discussion of the form factor and the experimental set up, results from measurements on spheres are presented and the procedure for determining the elastic parameters of spheres is described. Results are compared to previously published values for WC spheres. Also, the way the spheres are suspended is discussed. Next, measurements from rotated cylinders are presented and discussed. Summary and conlusion finishes the paper.

THE FORM FUNCTION

Scattering from spheres and cylinders is a "classic" subject and has received a substantial attention in the literature. The first study of sound wave scattering from elastic spheres and cylinders was given by Faran [1], and dealt with normally incident compressional waves on a submerged, elastic, isotropic and homogeneous sphere, or an infinitely long rod. A normal mode expansion technique was used, which since has become the basis of most later approaches, although various numerical techniques have been developed to perform the actual computations. An excellent review of scattering from elastic bodies in general is given in [2]. Since about 1980 scattering from spheres has become the basis of a standard method for calibrating ultrasonic transducers [3, 4, 5]. For this purpose spheres of Cu and WC (tungsten carbide with 6% of Co as binder) have become the mostly used targets, since their material properties are assumed to be predictable and stable with time.

Scattering from spheres is commonly expressed in terms of the form function, $f(\theta, ka)$, which is defined in terms of the ratio of the scattered pressure, $p_s(\theta, ka)$, and the incident (plane wave) pressure, p_0, at the sphere, at distances far from the sphere. Here ka is the dimensionless frequency in terms of the wave number, $k = 2\pi f/c$, and the radius, a, of the sphere. f is frequency of incident sound and c is wavelength in the surrounding medium (water). The angle θ is measured from the propagation direction of the incident wave.

Thus,

$$f(\theta, ka) = \left(\frac{2r}{a}\right)\left|\frac{p_s(r, \theta, ka)}{p_0}\right|. \tag{1}$$

The scattered pressure was found by Faran [1] by expanding the incoming wave and the two waves inside the sphere (compressional and shear) in spherical harmonics, and matching pressure and normal velocity at the surface. From this is obtained a set of linear algebraic equations whose solution is found by simple matrix manipulations. Faran's solution is essentially the "T-matrix" (transition matrix) for the elastic sphere. The form function for an infinitely long cylinder has the same form as Eq. (1), except that the geometric spreading goes as $\sqrt{2r/a}$. It contains the same features as that of a sphere but is simpler to interpret, and we therefore chose to use this as an example.

A typical back scattering form function ($\theta = \pi$) is shown in Figure 1 for an aluminum cylinder, with incident waves normal to the cylinder axis. At low frequencies $(ka < 1)$ we have Rayleigh scattering, followed by geometrical scattering. Here there is also interference with creeping waves (Franz waves) around the cylinder. At $ka \approx 4$ scattering starts to be dominated by modal resonances in the cylinder. Much effort has been made to interpret these resonances [6, 7, 8], and a full discussion of these is outside the scope of this paper. Briefly, the extent to which these modes get excited is related to how the incident wave couples to the eigenmodes. The dips seen in the form function occur at the modal resonances for much the same reason why absorption lines are seen in the spectrum of light passing through a gas. The wavelengths corresponding to exitation levels in the gas appear dark because this light is reradiated in all directions. If the gas is excited by other means (heating) these lines appear as bright. The width of the dips

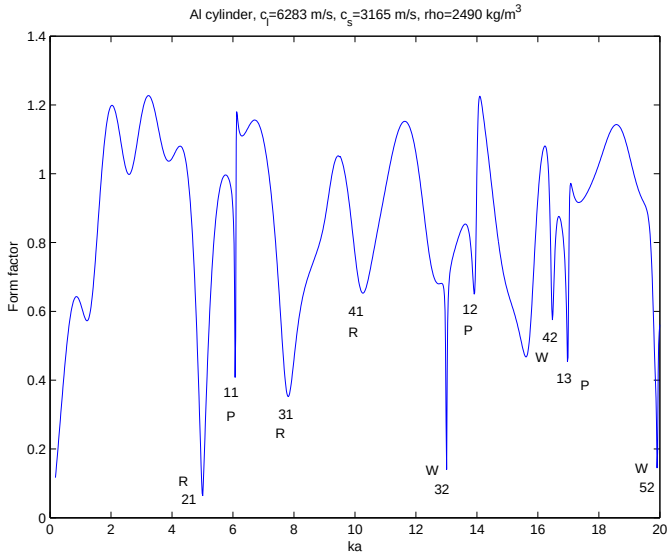

FIGURE 1. Form function for an aluminum cylinder. Indices refer to eigenvalues for the excited modes, letters to related wave type - see text.

is related to the efficiency of the coupling, and hence to the magnitude of scattering. At other directions these dips may become peaks.

Resonance scattering theory [9] states that the form function consists of two distinct parts: The first part varies smoothly with frequency and would be present even if the target was impenetrable to sound waves. The other part is the resonance spectrum which consists of a number of resonance peaks that coincide with the eigenfrequencies of the circumferential vibrations of the sphere or cylinder. Überall *et al.* [6] have interpreted the dips marked R in Figure 1 as associated with Rayleigh type surface waves propagating circumferentially around the cylinder, and the dips marked W to similar Whispering-gallery type waves. Also some weak dips associated with "breathing" waves are seen, marked P. The coupling of the latter is very weak, and acordingly the dips in the form function are narrow and shallow. Also, in the same figure, indices referring to the eigenvalues, *nl*, of the unloaded aluminum cylinder are given, where *n* is the modal number and *l* is the overtone number for each mode. The scattering directivity for each mode follows $\cos(n\theta)$.

The numerical code used in our simulations of the form factor is based on Faran's analysis, and programmed in MATLAB. The cylinder code was also programmed in C++. To evaluate the code, simulations were compared to various form functions published in the literature, and perfect agreement obtained. In these simulations no account was taken for losses, neither in the boundary layer about the target, nor inside the target. For targets of metal the losses are only marginal, but for softer materials like bone and plastic this may be of concern.

EXPERIMENTAL ARRANGEMENT

The experiment was based on mostly standard components. All vital instruments were controlled by a PC running Linux (Fedora) operating system, equipped with a GPIB-bus controller. The rotating table, with one arm for the hydrophone and another for the target, rotating about the same vertical axis as shown in Figure 2, was controlled from the parallell port of the same PC.

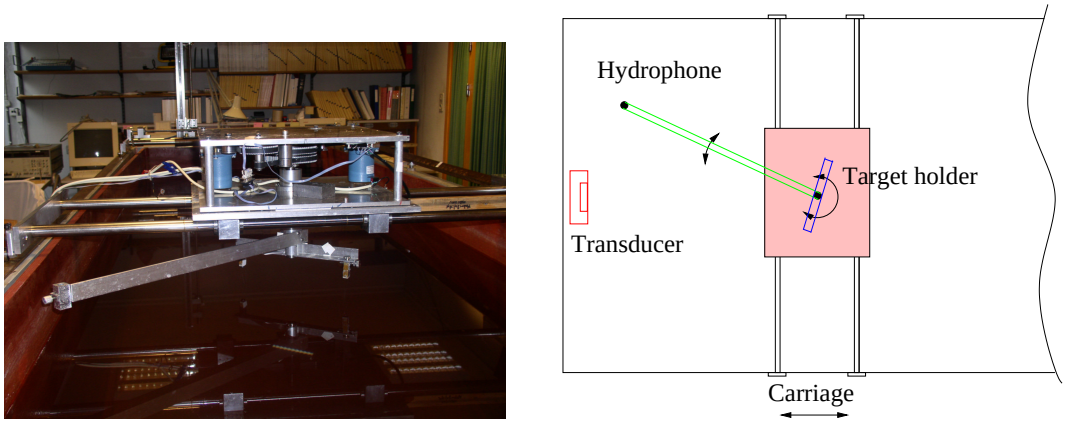

FIGURE 2. Left: Rotating table with two arms. Target barely visible: artificial fish backbone. Right: Principal lay out seen from above.

Signals from a function generator, HP33120, was passed through an ENI310L power amplifier to the sound source. For monostatic measurements a signal divider was used to prevent the strong transmitting signal to enter the receiving system. Signals from the hydrophone or tranceiver was digitized with a TDS220 oscilloscope, synchronized with the transmited signal. The tank dimensions were $1 \times 1 \times 4$ m^3. The target was located 1.3 m from the transmitter.

For high frequency measurements (700 - 1000 kHz) an air backed piezoceramic (PZT) disk of diameter 25.4 mm and resonant near 1 MHz was used as sound source, and a similar disk as hydrophone. For low frequencies (100-300 kHz) a composite tranducer borrowed from Simrad A/S (nominally a 200 kHz pinger) was used as source, and a Brüel & Kjær 8103 hydrophone as reciever for calibration purposes. In monostatic measurements the source also was used as the receiver.

In order to approximate a CW-situation tone bursts of 100 cycles were used. The received signal was averaged in the oscilloscope over 16 bursts in order to reduce random noise, and the whole sweep recorded for further analysis. For the cylinder rotation experiments signals at all frequencies in the scan were recorded at each step of rotation. In the final analysis a section of the stable region in each record was selected and the RMS-value computed. The limited size of the tank, and reflected sound radiated from the sides of the transducer sometimes caused strong stable signals to overlay the echoes from the target. The effect of this was removed by recording the signal without the target present, and subtract this deterministic signal from the target echo in the signal processing. This worked fine most of the time, except on a few occasions where the temperature in the tank changed during the measurement series, which often lasted for more than 10 hours.

MEASUREMENTS ON SPHERES

Suspension methods

4 different WC spheres of different sizes, used for standard calibration of echo sounders were borrowed from the Institute of Marine Research, Bergen (IMR). They came with a tight net of nylon gut (monofilament) knitted to each sphere, see Figure 4. Among our first measurements we rotated one of these spheres, 19.5 mm diameter, 180 degrees about a vertical axis, while the sound beam is horizontal, at frequency 860 kHz. The result was disturbing, as shown in Figure 3, left - red curve.

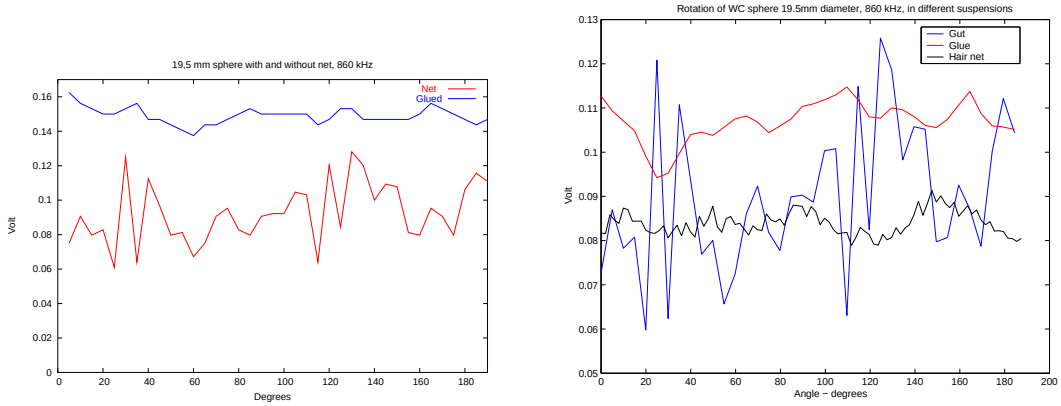

FIGURE 3. Rotation of suspended spheres. Left: Red curve = nylon net, Blue curve = bronze filament glued to sphere. Right: Blue = nylon gut, Red = glue, Black = hair net.

The sphere was kept in water for more than one week before the measurements were taken, in order to ensure that any air bubbles were dissolved. Similar results were measured with the other spheres as well. At this stage IMR allowed us to remove the nylon net on one sphere and try other means of suspension. Our first attempt was to glue a 50μm tungsten filament to the sphere with acrylic glue. The blob of glue was very thin, and made a negligible impact on the reflected signal. The result is shown in Figure 3, left, blue curve (the reason why it lies above the previous is that a stronger transmitted signal was used). The variations as the sphere is rotated are seen to be much smaller than previously. Unfortunately this type of suspension was not reliable, because after a few days in water the glue broke. Our next attempts were with a nylon hair net and a fine nylon stocking. Both of these gave improved results. In Figure 3, right, some examples are shown with hair net, glue, and nylon gut. The reason the curves are shifted vertically with respect to each other is because the spheres were not exactly in the same position. These measurements were taken with a bistatic arrangement, with the hydrophone at 170 degrees from the incident beam. Details of the suspension of spheres in nylon stocking and in nylon gut net are shown in Figure 4. The sphere in the stocking was photographed one year after the measurements were taken, and the stocking has become slightly damaged.

These results demonstrate that the influence of the suspension may be substantial, and for precision calibration this should be considered carefully. When sonars and echo sounders are calibrated the sphere is usually seen from above such that the same

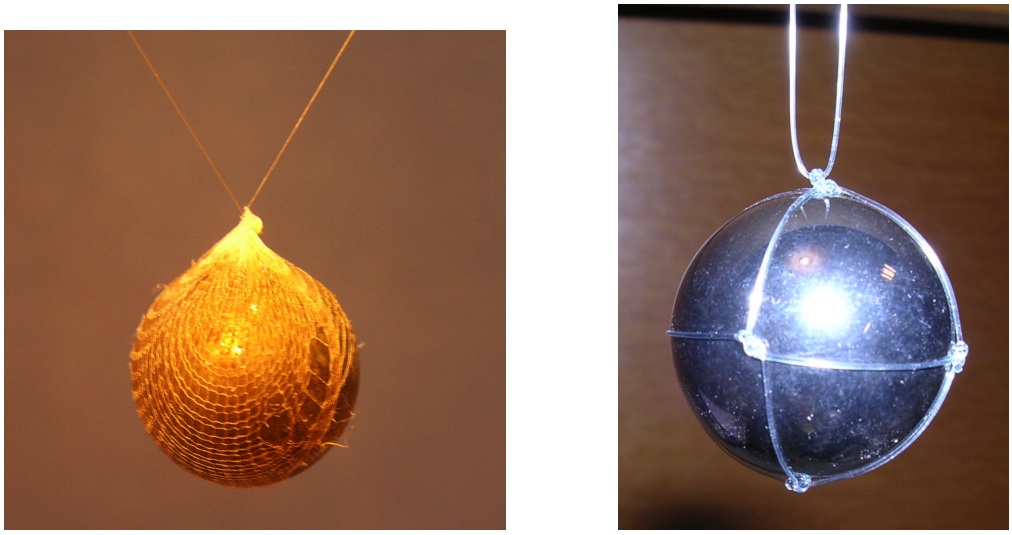

FIGURE 4. Suspended spheres. Left: 19.5 mm diameter sphere in fine threaded nylon stocking, Right: 19.5 mm diameter sphere in nylon gut net.

part of the net is exposed to the sound field irrespective of sphere orientation. In our measurements the sphere is seen from the side, and different parts of the suspension is exposed as the sphere is rotated. Thus, this case is more sensitive to the influence of the suspension. However, the fact that the variation can be so large indicates that the target strength of the sphere will be influenced by the nylon gut net, and not conform with the theoretical simulation, i.e. introducing errors when used for calibration.

Form factor

The measurements needed for finding the form factor are as follows. With a bistatic set-up the scattered signal from the sphere, V_s, is recorded with the hydrophone at an angle 170 degrees from the incident direction (10 degrees away from backward scattering), in the chosen range of frequencies. Next, the sphere is removed, the hydrophone is placed at the position of the sphere, and the received signal, V_h, is recorded in the same frequency range. This represents the free-field signal at the target. Since the frequency response of transmitter and receiver are the same in both cases, they will cancel out when we take the ratio of the two signals. Thus, the form factor at 170 degrees is found by

$$f(170,ka) = (\frac{2r}{a})|\frac{V_s(170,ka)}{V_h(ka)}|. \tag{2}$$

at each frequency (here ka). The form factor measured on one 19.5 mm diameter WC sphere in nylon stocking is shown in Figure 5 (these figures are "uncalibrated" in the sense that the geometrical correction is not included).

The frequencies of the minima in the form factors, annotated in the panels, correspond very well, but the level of the intermediate sections differ somewhat. In the next figure

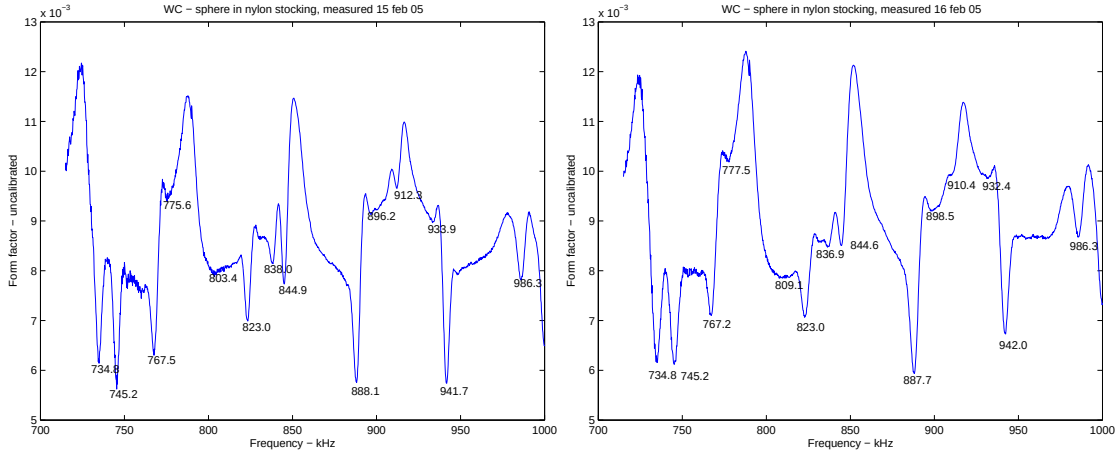

FIGURE 5. Measured form factor on WC sphere suspended in nylon stocking, 19.5 mm diameter. The right panel is measured one day later, after rotating the sphere 90 degrees.

the two measurements are superimosed and shown together with the form factor computed with parameters from MacLennan [3], which were the first we discovered in the literature.

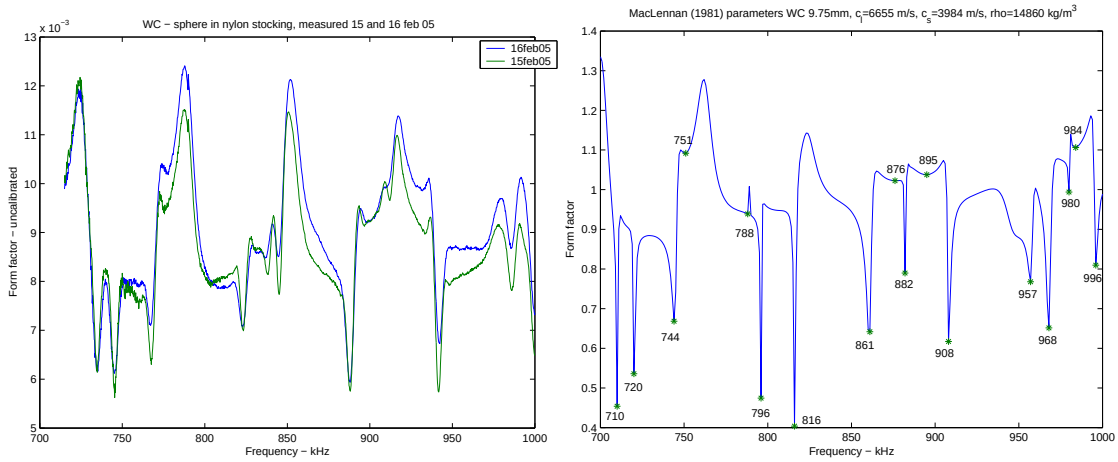

FIGURE 6. Left: Superimposed measured form factors on WC sphere suspended in nylon stocking. Right: Simulations for the same sphere using MacLennan's [3] parameters.

It is possible to recognize some main features, but they are not very similar, and the position of the dips do not correspond in frequency. In order to obtain better correspondance we tried to vary the two wave speeds in the WC sphere, and determined the density of the sphere by weighing. In this way a better, but not perfect, correspondance was obtained. Different approaches for parameter inversion were considered, like using genetic algoritmhs or simulated annealing. The problem lies in obtaining a relevant cost function. Attempts based on comparing all parts of the form functions step by step does not guarantee a good result, since the measurements obviously contains "errors" in the magnitude in areas between the dips. A better approach is to minimize the differences between the frequencies of the dips in the two form functions. The dips are easily lo-

cated by examining changes in the sign of the derivated form function. However, it is not easy to automize the cost function, because while the parameters are varied some of the dips may disappear or new ones appear, causing confusion in the order of comparison. Finally a semi-automatic process was deviced. A set of parameters which gave a form function not too distant from the measured one was chosen as a starting point. These parameters were $c_L = 6887$ and $c_S = 4135$ m/s, for the compressional wave speed and the shear wave speed, respectively. Next, c_L and c_S were varied in steps of 10 m/s about these values, and the location of the dips were recorded. In Figure 7 (right panel) the locations of the dips are plotted as c_S (inner loop) and c_L (outer loop) are varied (when the color of the dips change, one of them has disappeared or a new appeared).

The vertical scale in the map is frequency, and at the right hand side the individual dips are identified according to the typical form factor shown in the left panel. The horizontal scale is run-number, which identifies the actual parameters used. Thus, at first c_L is fixed and c_S varied 11 steps, i.e. 5 steps on each side of the central value. Then c_L is increased 10 m/s, and the process repeated. It is evident that the different dips vary with wave speeds by different amounts. Most dips depend strongly on c_S, but in particular the one marked E' is almost insensitive the value of c_S, but varies slowly with c_L. This facilitates the fixation of a good value of c_L by finding the index which gives the best match between the measured and the simulated frequency for dip E'. This procedure results in $c_L \approx 6837 \pm 10$ m/s. Next, two dominant dips, A and J, which vary strongly with c_S, were used to locate the shear velocity to be near 4131 m/s. Finally, a systematic search by varying both wave velocities in small steps, and minimizing the cost function $ss = \sqrt{(\sum_j (fm_j - fs_j)^2)}$, where the index j runs over the dips marked A, B, C, D, E, E', F, H, I, J and K in Figure 7, left panel. Here fm_j is the measured frequency of dip j and fs_j the corresponding simulated one. The best match determined in this way is $c_L = 6845$ m/s and $c_S = 4132$ m/s. The cost function detects easily variations in ± 1 m/s in the wave speeds, so it should be possible to determine these to such an accuracy. However, the accuracy in the determination of the frequency of the measured dips limits accuracy of the wave speeds to ± 2 m/s. Table 1 compares the frequencies of measured and simulated "best match" dips. The correspondance is quite satisfacory.

The next question is how representative these new parameters are for other WC spheres. Figure 8 shows measurements on a 38.05 mm sphere, and simulations based on our new parameters. Obviously, the correspondance is not as good as for the sphere used for determining the parameters. This is particularly seen in the dips at the highest frequencies. A much better fit for the large dips is found with the parameters presented in [10], see Table 2. This form function is shown in Figure 9.

Comparisons are also made to measurements on WC spheres in a previous experiment. In that case 3 spheres from the same batch were investigated. The spheres were naked and suspended on a nylon stocking stretched across a circular frame. A monostatic set up was used, with the sound beam directed vertically from the bottom of a small tank. The measured form functions were almost identical for the three spheres, and one example is shown in Figure 10.

The best fit of parameters in this case is with parameters published by Gerlich *et al.* [11].

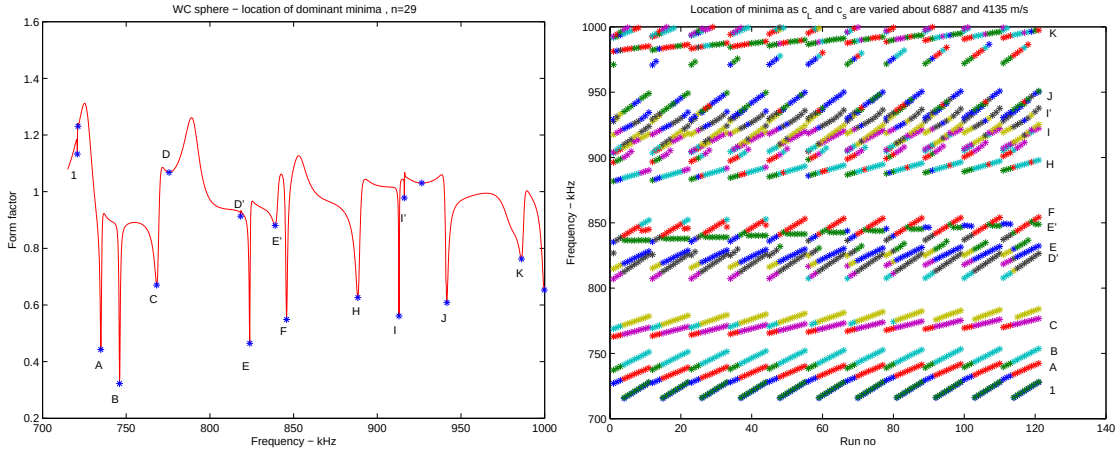

FIGURE 7. Left: Simulated form factor with dominant dips named, Right: Map of dominant dips - c_L and c_S varied.

Discussion

It may be argued that the difference in wave speeds in WC spheres with 6% Co binder are only marginal. This argument may be correct at low frequencies and small sphere radia, i.e. $ka < 5$. However, if the spheres are going to be used for high precision calibration of acoustic transmitters or receivers, in particular at frequencies above 500 kHz, it is important to know the precise parameters of the sphere material. One of the reasons why WC was chosen as a promising material for such spheres was that the parameters were considered to be well controlled during the production. These measurements show that this is not strictly correct, and that spheres from different batches vary in

TABLE 1. Comparison of measured dip frequencies and simulated ones with “best match" parameters. Frequency in KHz.

Dip	Measured	Best match
A	734.8	734.4
B	745.2	745.6
C	767.5	768.0
D	775.6	775.4
E	823.0	823.2
E’	838.0	838.8
F	844.9	845.2
H	888.1	888.0
J	941.7	941.0
K	986.3	985.8

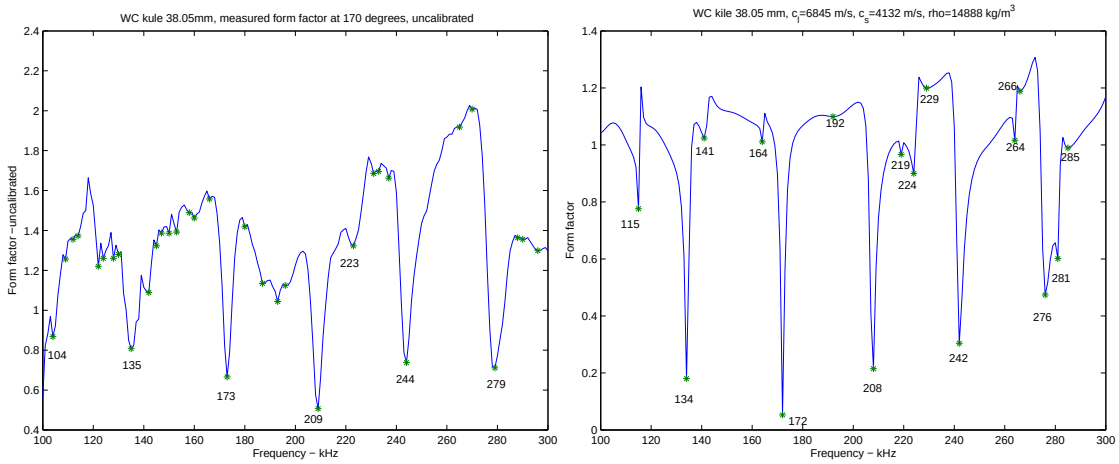

FIGURE 8. WC sphere 38.05 mm diameter, Left: Measured form factor, Right: Simulations, our "best fit"parameters.

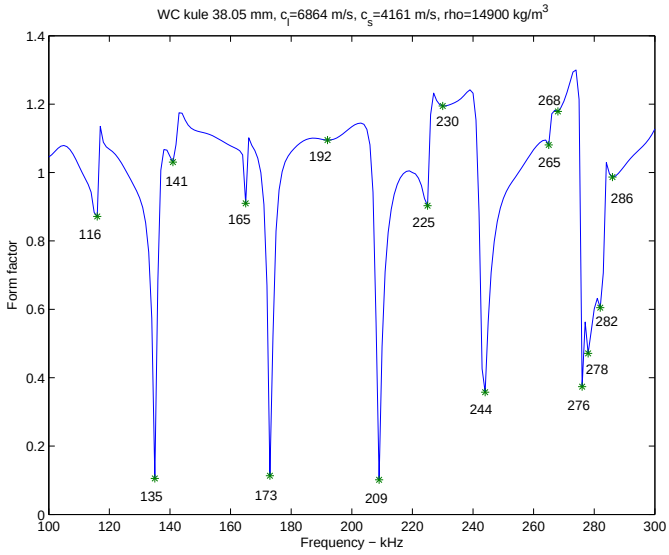

FIGURE 9. WC sphere 38.05 mm diameter, simulations, parameters from [10].

both compressional and shear wave speeds. Thus, for calibration purposes each batch of spheres should have its parameters determined on an individual basis, and preferrably each sphere.

Another matter to consider is ageing. To which extent this takes place for WC we do not know, but in many alloys and even in pure substances, the mechanical properties are known to change with time after manufacture. In particular this is the case for Cu, even in very pure conditions. Recall that spheres of Cu are also much used for calibration purposes. Thus, in order to secure precision of calibration ageing of the parameters of WC and Cu should be investigated. Finally, the temperature dependence of the wave speeds should be investigated, in order to be able to correct for changes in the form

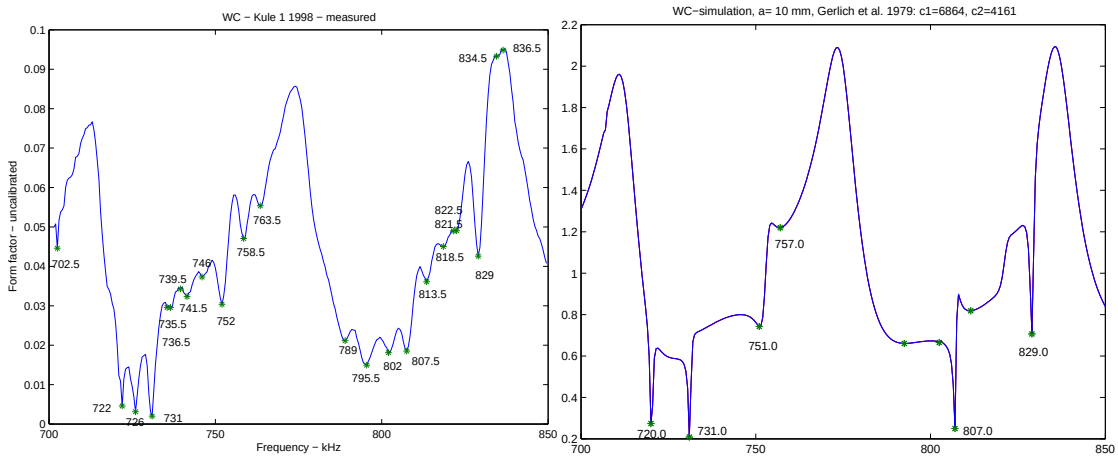

FIGURE 10. WC sphere 10.0 mm diameter, Left: Measured form factor, Right: Simulations, Gerlich *et al.'s* parameters [11].

TABLE 2. Table of WC parameters found in literature and our best match.

Authors	c_L [m/s]	c_S [m/s]	ρ [kg/m^3]
MacLennan [3]	6655	3984	14860
Gerlich *et al.* [11]	6864	4161	14900
MacLennan & Dunn [10]	6853	4171	14900
Our best match	6845	4132	14888

function with temperature. Both of these topics lies outside the scope of the present investigation.

MEASUREMENTS ON CYLINDERS

Some measurements were made on short cylinders in order to investigate the directivity pattern caused by the finite length. Presented here are measurements made on aluminum cylinders of diameter 8.35 mm and length 100.0 mm and 73.45 mm, respectively, with straight cut ends. They were suspended horizontally in fine nylon filaments tied around each end and rotated about a vertical axis through their mid points. The actual composition of the aluminum alloy is unknown. Figure 11 shows the measured (uncalibrated) broadside form function and the simulated one with parameters that match the dominant dip. The latter is easily identified as dip 21 in Figure 1. The location of dip 21 turns out to be almost insensitive to the value of c_L, so only c_S can be determined from this form factor, yielding $c_S = 3165 \pm 5$ m/s. Most tables giving elastic parameters for aluminum specify Poisson's ratio, $\sigma = 0.33$, resulting in $c_L = 6283$ m/s.

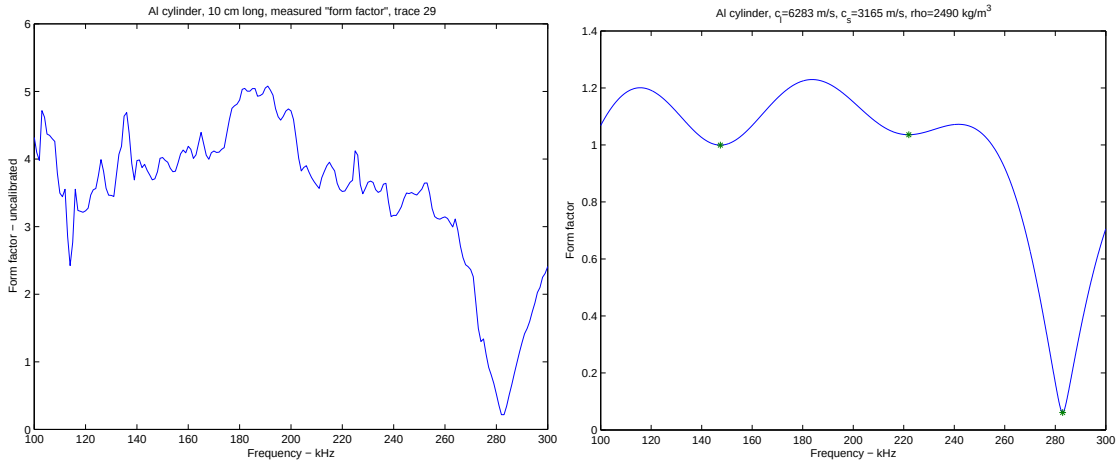

FIGURE 11. Measured (left) and simulated (right) form factor of 10 cm cylinder (broadside).

If the cylinder pulsates uniformly the radiated sound obtains a radiation pattern like a line array, i.e. given by the sinc-function

$$D(\alpha) = \frac{\sin(\frac{1}{2}kL\sin\alpha)}{\frac{1}{2}kL\sin\alpha}, \tag{3}$$

where L is cylinder length and k the wave number in the surrounding fluid. This is what one should get if the cylinder is oriented broadside, and the incident waves are plane. In a monostatic set-up an incidence angle of α with respect to normal incidence would cause the phase speed of the incident wave along the cylinder to be $c_p = c/\sin(\alpha)$, and the reflected wave to be centered on the angle α at the other side of the normal (Snell's law). For the short cylinder at oblique incidence, α, this means that the sound scattered back to the transmitter gets a sinc function directivity with argument $\frac{1}{2}kL\sin(2\alpha)$. A verification of this is shown in the scatter map in Figure 12. Here the target strength is mapped as a function of incidence angle -30 to $+30$ degrees [horizontal axis] - and frequency [vertical axis]. The color represents the amplitude (target strength). In the main lobe, i.e. the central part, the form function with the big dip at 283 kHz is easily recognized. The tiny pattern symmetric about the central part are the sidelobes caused by the sinc-function. On the right hand side some zeros of the sinc-function, simulated with the actual length L of the cylinder, have been overlayed, and they match this pattern very well.

However, the strong lobes located at about 18 degrees to each side of the main lobe, almost independent of frequency, were a great surprise. A closer examination shows that they tend to move towards greater angles at frequencies above about 250 kHz. Another pattern of lobes, although weaker, is seen to appear for frequencies above 230 kHz, where the lobes seem to emerge from the central lobe.

The short cylinder shows exactly the same patterns, Figure 13, and the new sets of lobes appear at the same angles and frequencies.

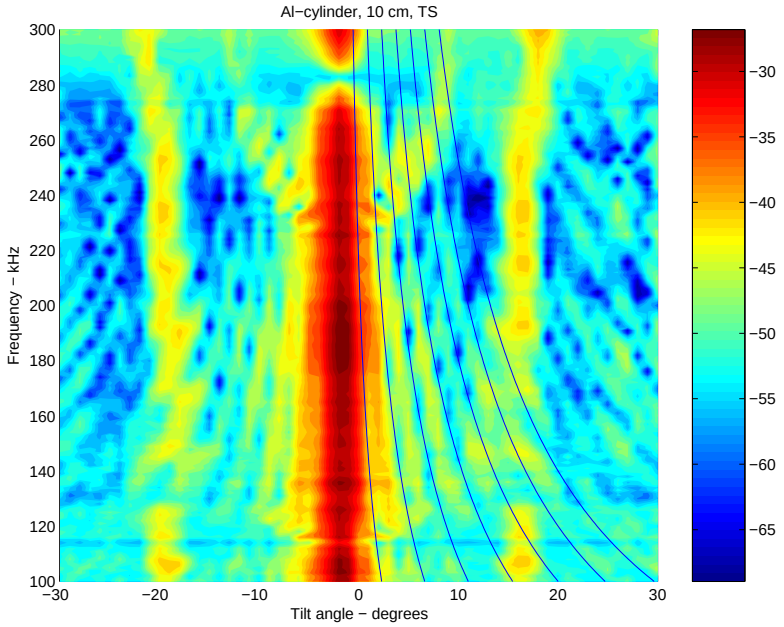

FIGURE 12. 10 cm cylinder overlayed locations of zeros of sinc($\frac{1}{2}kL\sin\{2\alpha\}$).

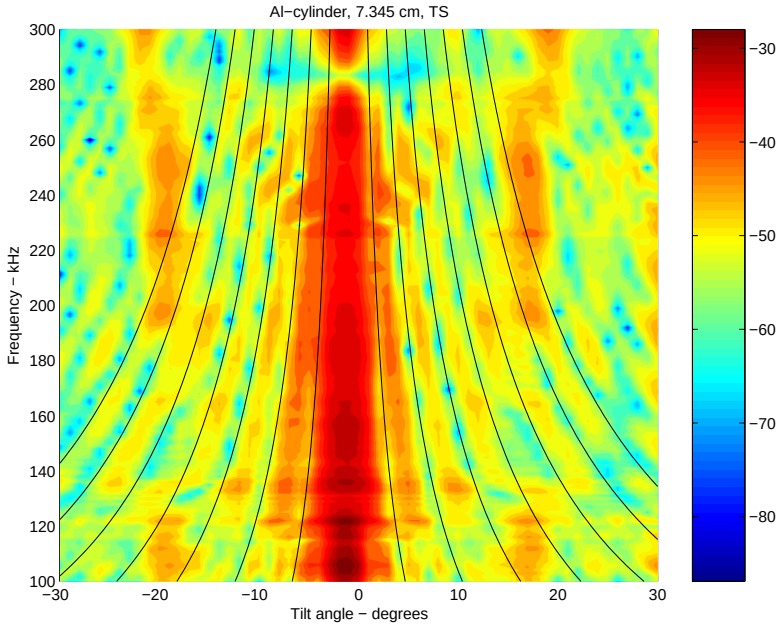

FIGURE 13. 73.45 mm cylinder overlayed locations of zeros of sinc($\frac{1}{2}kL\sin\{2\alpha\}$).

Discussion

So far we have not been able to find previously published records of similar measurements. The length of the cylinder does not seem to influence the location of the lobes.

For the long cylinder the mean angle between 100 and 240 kHz is 18.2 ± 0.3 degrees and for the short 18.5 ± 0.4 degrees. This is consistent with a radiation from a wave propagating along the cylinder with phase speed $v = c/\sin(18.2) = 4777 \pm 100$ m/s, where the sound speed in the water is 1492 m/s (physiological salt water). The most relevant wave to compare this to is the first symmetric Lamb wave in an unloaded bar (in many text books referred to as longitudinal wave in bars), $v_L = c_s\sqrt{2(1+\sigma)} = 5162$ m/s, with c_S as above. This is somewhat higher than the measured one, but still not very far off. Note that if this is the cause of the observed lobes, the Lamb waves must propagate in the direction opposite the projection of the incident wave on the cylinder, and must have been reflected from the end of the cylinder. Thus, one should expect a standing wave to be present on the cylinder surface. The fundamental resonance frequency of symmetric Lamb waves for the $L = 10$ cm cylinder is found by $L = \lambda/2$, resulting in $f_1 = 25.81$ kHz . The duration of the tone bursts should be long enough to set up a standing wave pattern, since the fundamental period of the symmetric Lamb wave is $1/f_1 = 39\mu s$, and the burst length is 100 periods, which is $500\mu s$ at 200 kHz. However, the only evidence of fluctuations along the lobes (as a function of frequency) in the measured field seems to be due to interference with the "sinc" sidelobes. It is also puzzling that the main lobe does not show any sign of the presence of the second mode near 230 kHz, conf. Figure 11.

A more detailed study of the lobes leads to dispersion relations for two different modes. To start with, a plot of v/c as a function of (dimensionless) frequency, found by putting $v/c = 1/\sin\theta$, is presented in Figure 14 for both modes. Mode 1 (red curve) refers to the lobe at 18 degrees, and Mode 2 to the one emerging at 230 kHz. The frequency axis has been made dimensionless by using the actual cylinder radius a and sound speed c in water, i.e. ka, where $k = \omega/c$. It is interesting to note that the

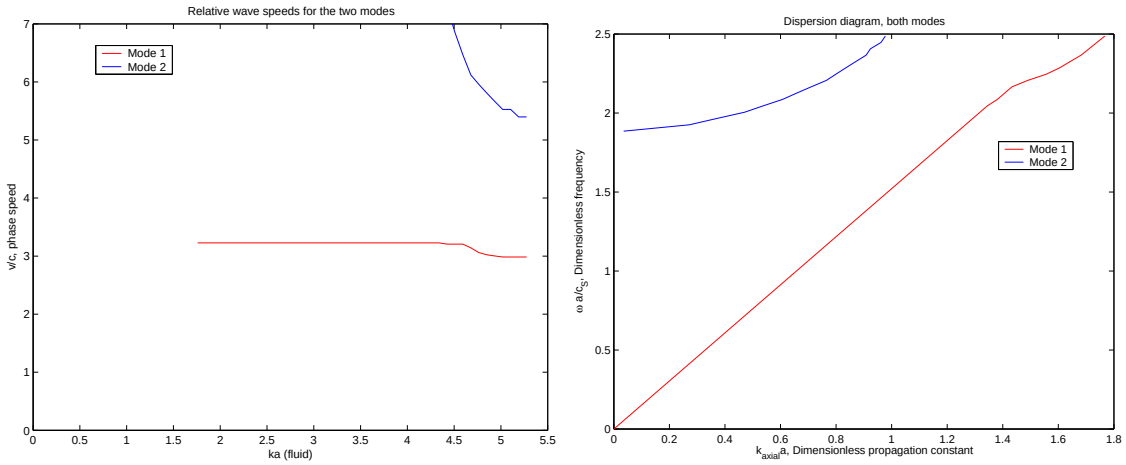

FIGURE 14. Dispersion curves for the two modes. Red: Mode 1, Blue: Mode 2. Left: v/c versus ka(fluid), Right: Dimensionless frequency $\omega a/c_S$ versus $k_{axial}a$.

shape of these of curves has a strong likeness with plots of mode L(0,1) and F(1,2) in Fig. 14 in [2] for an aluminum cylinder, where these modes are referred to as the "first $m = 0$ axisymmetric" and "second m=1 flexural " modes of an infinite aluminum cylinder, repectively, i.e. the first symmetric and the second asymmetric Lamb mode in

the termonology adopted above. It appears that the low frequency value of the phase speed relative to the sound speed in water of Mode 1, v_1/c, is just above 3 in [2] while our measurements gives 3.2. Furthermore, v_1/c starts to decrease at about the same values of ka. The high frequency limit is approximately the Rayleigh wave speed (in an elastic half space), which is $0.93c_S$, or $v_1/c = 1.98$ for our case. The frequencies used in our experiment are not high enough to verify this limit.

Mode 2 is a bit harder to identify, but seems to fit numerically close to the curve of F(1,2) in [2]. It could, however, also match other modes, namely L(0,2), or F(2,1), i.e. the "second $m = 0$ symmetric mode" and the " first $m = 2$ asymmetric mode". In order to investigate this further a dispersion diagram of the regular type, i.e. frequency as a function of (axial) wavenumber, is plotted for the two modes, as shown in the right panel in Figure 14. This is obtained by plotting dimensionless frequency ($\omega a/c_S$) against $k_{axial}a = \omega a/v = (\omega a/c)\sin\theta$ for the two modes (note that Mode 1 has been extended to zero frequency artificially by assuming a constant wave speed at low frequencies). This plot may be compared numerically to Fig. 12 in [12], which presents dispersion curves for various longitudinal and flexural modes in a cylinder having $\sigma = 0.33$. I appears that Mode 2 matches the F(1,2) mode closely, and differs clearly from modes L(0,2) and F(2,1). Also the L(0,1) fits well the dispersion curve for Mode 1. Thus, there is a strong evidence that Mode 1 is related to the L(0,1) mode and Mode 2 to the F(1,2) mode. It should, however, be kept in mind that the curves presented in [2, 12] are computed for unloaded infinitely long cylinders, not short cylinders embedded in water as used in this experiment.

SUMMARY AND CONCLUSIONS

Measurements are made on the form function of WC spheres. It is found that the form function depends strongly on the exact compressional and shear wave speed in the sphere, and that these need to be determined for the particular sphere if the sphere is to be used in precision calibration of acoustic instruments. The material parameters may vary from batch to batch of WC spheres, and may differ from values found in the literature. One method to determine these parameters from the measured form function is demonstrated. It is also found that the method of suspension of the spheres influences strongly on the reflected signal, and should be considered seriously when precision calibration is needed.

Measurements are also made on scattering of sound waves from short cylinders of aluminum as they were rotated. It is found that in addition to the sidelobes due to the finite length of the cylinder two sets of strong lobes are present, which we have not seen described in the literature. One of these is largely independent of frequency in the range 100 – 300 kHz, and is identified as radiated by a wave propagating along the cylinder and related to a symmetric Lamb type wave in an unloaded cylinder. The second set of lobes depends strongly on frequency and is similarly found to be related to an asymmetric Lamb wave. Dispersion curves for the two modes are presented. For the cylinders and frequency range at hand the form function allows determination of the shear wave speed, but the compressional wave speed has to be determined using the nominal Poisson's ratio.

ACKNOWLEDGMENTS

We thank Rolf Korneliussen at the Institute of Marine Research, Bergen, for providing the calibration spheres, and for lending us the Simrad transducers.

REFERENCES

1. J.J. Faran Jr. "Sound scattering by solid cylinders and spheres", *J. Acoust. Soc. Am.* **23**, 405-418 (1951).
2. R.H. Hackman, "Acoustic scattering from Elastic Solids", in *Physical Acoustics Vol XXII, Underwater Scattering and Radiation,* edited by A.D. Pierce and R.N. Thurston, Academic Press, 1993.
3. D.N. MacLennan,"The theory of solid spheres as sonar calibration targets", Scottish Fisheries Research Report No. 22, (1981).
4. K.G. Foote, "Optimizing copper spheres for precision calibration of hydroacoustic equipment",*J. Acoust. Soc. Am.* **71**, 742-747 (1982).
5. K. G. Foote and D. T. I. Francis, " Scheme for parametric sonar calibration by standard target", Oceans 2005 MTS/IEEE Conference Proceedings, electronic document no. 050304-143, 6 pp.
6. H. Überall, L.R. Dragonett and L. Flax, "Relation between creeping waves and normal modes of vibration of a curved body", *J. Acoust. Soc. Am.* **61**, 711-715, (1977)..
7. X.-L. Bao, H. Cao and H. Überall, "Resonances and surface waves in the scattering of an obliquely incident acoustic field by an infinite elastic cylinder", *J. Acoust. Soc. Am.* **87**, 106-110 (1990).
8. Y. Fan, F. Honavar, A.N. Sinclair and M.-R. Jafari, "Circumferential resonance modes of solid elastic cylinders excited by obliquely incident acoustic waves", *J.* Acoust. Soc. Am. **113**, 102-113 (2003).
9. L. Flax, L.R. Dragonette and H. Überall, "Theory of resonance excitation by sound scattering",*J. Acoust. Soc. Am.* **63**, 723-731 (1978).
10. D.N. MacLennan and J.R. Dunn, "Estimation of sound velocities from resonance measurements on tungsten carbide calibration spheres, *J. Sound. Vib.* **97**, 321-331 (1984).
11. D. Gerlich and G.C. Kennedy, "Elastic moduli and their pressure derivates for tungsten carbide with different amounts of cobalt binder", *J. Appl. Phys.* **50**, 3331-333 (1979).
12. T.R. Meeker and A.H. Meitzler, "guided wave propagation", in *Physical Acoustics Vol I - part A, Principles and methods,* edited by Warren P. Mason, Academic Press, 1964.